QUARTERLY OF APPLIED MATHEMATICS
VOLUME XLVI, NUMBER 4
DECEMBER 1988, PAGES 637–663

THE FIGURE-OF-8 LIBRATIONS OF THE GRAVITY GRADIENT PENDULUM AND MODES OF AN ORBITING TETHER*

BY

PETER J. MELVIN

Naval Research Laboratory, Washington, D. C.

Abstract. An algorithm is presented for the Hill–Poincaré analytical continuation of the out-of-plane normal mode of the gravity gradient pendulum. The Poincaré–Lindstedt solution employs 17 Poisson series and 24 recursion relations and was evaluated to the 50th order on a CRAY. The trajectories of the nonlinear normal modes are figures-of-8 on the unit sphere which can be computed nearly to the orbit normal. Numerical integrations indicate further that 1) initial conditions computed at the nadir can be used to generate figures-of-8 over the pole, 2) the single hemispherical figures-of-8 appear to be stable at large amplitudes, and 3) the gravity gradient pendulum has chaotic solutions. A theory is developed for the linear normal modes of a tethered satellite, and the eigenvalues are found for the rosary tether.

1. Introduction. The gravity gradient pendulum is not only the simplest idealization but also the fundamental mode of a tethered satellite. The equations of motion are derived in spherical coordinates from the components of Hill's equation for relative satellite motion [1, p. 289] in a circular orbit by the constraint that a pair of point mass satellites remain a fixed distance apart. The motion of an orbiting tether made of $N+1$ point masses is governed by N coupled, vector Hill equations, and for a tether without elastic or frictional properties the interparticle forces are obtained from the radial components of the Hill equations by constraining the particles to be a fixed distance apart. The theory of an orbiting, segmented tether is thus a natural generalization of its own simplest idealization.

In this paper a hitherto overlooked, large amplitude, two degree of freedom, periodic libration of the gravity gradient pendulum is constructed by the method of Poincaré–Lindstedt. In Hughes [2] there is an extensive discussion of analytical solutions to the equations of satellite attitude dynamics, but no mention is made of the hourglass shaped, periodic motion out of the orbital plane. The first step in the production of the higher nonlinear modes of an orbiting tether is the determination of the linear normal modes. In the last section of this paper a theory is presented for

*Received May 7, 1987.

a tether made of N segments, and the eigenvalues are given for the case of a rosary tether.

Although the terminology is recent, the existence of nonlinear normal modes in mechanical systems has long been known. Birkhoff [3, pp. 139–140] defines: "The method of analytical continuation of Hill and Poincaré starts with a known periodic motion and then obtains an analytic continuation of it with variation of a parameter". Contemporary studies of nonlinear normal modes begin with Rosenberg [4]. The author's interest comes from the pulsation theory of variable stars, Melvin [5]. There is interest in these solutions among mechanical engineers with the studies of Rand [6], and Month and Rand [7], and applied mathematicians with Pecelli and Thomas [8]. In physics there is the work of Nejoh [9] and Ferguson, Flaschka, and McLaughlin [10]. The term is also used by meteorologists, see, for example, Briere [11].

The construction of the Poincaré–Lindstedt solution described in Melvin [12] approaches the problem in one dimension, but nonlinear normal modes are far more difficult with the coupling of several degrees of freedom. In the study of periodic variable stars a vector differential equation of the form $y'' = F(y)$ describes the time dependence of the eigenfunction amplitudes. But from Birkhoff [3] nonlinear normal modes are possible in the general dynamical system governed by $y' = F(y)$. The distinction comes in several dimensions with what Birkhoff [3, p. 18] called "nonenergic systems." Both classes of problems describe motion in a potential, but the latter includes potentials in rotating coordinates such as the three-body problem or systems with gyrostatic or magnetic forces.

The approach is first to find the general form of the series solution of a nonlinear differential equation by examination of the lowest-order nonlinear terms. Then a consistent system of recursion relations are derived from the exact equations for the coefficients of the postulated series. For nonlinear systems the solution to the recursion relations is usually so involved that it cannot be carried out by hand beyond the first few steps, and a digital computer is used to generate higher-order approximations. Because the results cannot be improved further, the ideal situation is to produce the coefficients as rational fractions. The length of the relatively prime integers composing the fractions limit these approximations to only a few orders higher than those obtained by hand. Floating point representation of unknown precision is necessary for higher-order approximations.

Most modern analytical solutions to nonlinear differential equations use formula manipulation programs such as the commercially available MACSYMA or privately developed programs such as Dasenbrock's FORTRAN algebra [13] or Deprit's MAO [14]. This author prefers, however, the approach of analytically manipulating the series before turning to the computer.

The libration of the gravity gradient pendulum in the orbital plane is governed by a single nonlinear oscillator equation which is equivalent to the simple pendulum equation. In the nonlinear regime the out-of-plane normal mode differs from the in-plane mode because it requires both degress of freedom for its description. The trajectory of the in-plane normal mode is just an arc segment on the equator of the unit sphere, but the trajectory of the nonlinear normal mode out of the orbital plane

is best described as a *figure-of-8*. The figures-of-8 generated analytically in this paper bear a striking resemblance to the purely numerical results of Bray and Goudas [15].

The analytical continuation to large amplitude of the normal mode perpendicular to the orbital plane has led to several interesting results. First, the figure-of-8 is traversed only in one direction. Birkhoff [3] notes the failure of time reversal invariance in systems with non-energic forces. Second, as the amplitude is increased, the sign of the first integral changes without a change in the morphology of the solution. The dynamically bound, hyperenergetic solutions are only possible for a nonlinear normal mode described by two degrees of freedom. Third, numerical integrations suggest stability with trajectory bands of 10 degrees about the figure-of-8 for single hemispherical, hyperenergetic solutions. Fourth, although the present formulation produces reasonable polynomial approximations for amplitudes almost to the orbital normal, initial conditions obtained from the same Poincaré–Lindstedt solutions indicate that there are figure-of-8 trajectories over the pole.

The generation of the figure-of-8 libration is complicated. All results have been checked by numerical integration which has been checked in turn by the constancy of the first integral. During the process of validation of the numerical integrator for a variety of initial conditions, it became apparent that there is another large amplitude behavior of the gravity gradient pendulum of interest to applied mathematicians, namely, chaotic solutions. Most numerical solutions appear to be space filling but are limited to curvilinear regions much smaller than allowed by the first integral. The chaotic solutions are characterized by filling a much larger portion of the zero velocity surface.

2. Equations of motion. For a pair of satellites whose center of mass has a circular orbit, the Hill equation for the displacement of one satellite from the other is

$$\frac{d^2\boldsymbol{\rho}}{dt^2} + n^2\boldsymbol{\rho} - 3n^2\hat{\mathbf{R}}(\boldsymbol{\rho}\cdot\hat{\mathbf{R}}) = \mathbf{f}, \tag{2.1}$$

where $\hat{}$ denotes a unit vector, $\boldsymbol{\rho}$ is the displacement of one satellite from the other, $\mathbf{R}$ is the displacement of the center of mass from the center of the Earth, $n = \sqrt{GM/R^3}$ is the mean motion of the center of mass, and $\mathbf{f}$ is the interparticle acceleration. The Hill equation [1] was invented to study the motion of the moon and enjoyed considerable attention during the 1960's with the rendezvous studies of the Apollo missions. It is called the Euler–Hill equation in Hughes [2, p. 292, Eq. (37)] and the Clohessy–Wiltshire equation by Vassar and Sherwood [16, p. 241, Eq. A7] where a derivation from Newton's laws is found. It now resurfaces in the study of tethers.

Introduce a spherical coordinate system located at the center of mass, measure the intersatellite longitude λ in the orbital plane from the center of mass direction $\hat{\mathbf{R}}$ in a right-handed sense, measure the intersatellite latitude φ out of the orbit plane, positive toward the angular momentum vector of the orbit. The spherical components

of the equation of motion (2.1) are then

$$\frac{d^2\rho}{dt^2} - \rho\left\{\left[\left(n+\frac{d\lambda}{dt}\right)^2 + 3n^2\cos^2\lambda\right]\cos^2\varphi + \left(\frac{d\varphi}{dt}\right)^2 - n^2\right\} = f, \tag{2.2a}$$

$$\rho\frac{d^2\varphi}{dt^2} + 2\frac{d\rho}{dt}\frac{d\varphi}{dt} + \rho\left[\left(n+\frac{d\lambda}{dt}\right)^2 + 3n^2\cos^2\lambda\right]\sin\varphi\cos\varphi = 0, \tag{2.2b}$$

$$\left[\rho\frac{d^2\lambda}{dt^2} + 2\frac{d\rho}{dt}\left(n+\frac{d\lambda}{dt}\right) + 3n^2\rho\sin\lambda\cos\lambda\right]\cos\varphi - 2\rho\frac{d\varphi}{dt}\left(n+\frac{d\lambda}{dt}\right)\sin\varphi = 0. \tag{2.2c}$$

If the interparticle force is such that the particles are constrained always to be the same distance apart (ρ =constant), then the angular equations become

$$\frac{d^2\varphi}{dt^2} + \left[\left(n+\frac{d\lambda}{dt}\right)^2 + 3n^2\cos^2\lambda\right]\sin\varphi\cos\varphi = 0, \tag{2.3a}$$

$$\left(\frac{d^2\lambda}{dt^2} + 3n^2\sin\lambda\cos\lambda\right)\cos\varphi - 2\left(n+\frac{d\lambda}{dt}\right)\frac{d\varphi}{dt}\sin\varphi = 0. \tag{2.3b}$$

The first integral of the system is

$$\left(\frac{d\varphi}{dt}\right)^2 + \left[\left(\frac{d\lambda}{dt}\right)^2 - n^2 - 3n^2\cos^2\lambda\right]\cos^2\varphi = -4n^2C^2, \tag{2.4}$$

where C is a constant of integration. This integral is derived from the Lagrangian by the method shown in Symon [17, p. 383, Eq. (9-126)] or Goldstein [18, p. 53, Eq. (2-50)]. Symon notes that the integral does not have to be the energy of the system, but Goldstein identifies it with the energy. Whether or not it is the energy, it is definitely the Hamiltonian for the gravity gradient pendulum which is given by Hughes [2, p. 294, Eq. (12)].

Any system described by (2.3) is called a gravity gradient pendulum. Equations (2.3) have the stable equilibrium solution $\varphi = \lambda = 0$ which corresponds to the line joining the two masses pointing at the center of the Earth. The unstable equilibrium solutions $\varphi = 0$, $\lambda = \pi/2$ and $\varphi = \pi/2$, λ =constant correspond respectively to lines tangent and perpendicular to the orbit of the center of mass.

The equations of motion for the gravity gradient pendulum (2.3) are scale invariant, independent of the mass ratio at this order, and correct to the first order in the ratio of ρ/R. As noted by Hughes [2, p. 296], "... as far as gravity gradient torque is concerned, a dressmaker's pin has the same motion as a lodge-pole."

2.1. *Linear normal modes and zero velocity surfaces.* Expansion about the stable equilibrium of the system (2.3) to some of the lowest-order nonlinear terms yields

$$\frac{d^2\varphi}{dt^2} + 4n^2\varphi = -2n\varphi\frac{d\lambda}{dt} + \frac{8}{3}n^2\varphi^3, \tag{2.5a}$$

$$\frac{d^2\lambda}{dt^2} + 3n^2\lambda = 2n\varphi\frac{d\varphi}{dt}. \tag{2.5b}$$

With the neglect of the nonlinear terms, this system is completely integrated by the linear normal modes

$$\varphi = a\cos(2nt), \tag{2.6a}$$

$$\lambda = b\cos[\sqrt{3}n(t - t_0)], \tag{2.6b}$$

where a, b, and t_0 are the three constants of integration. Because the system is autonomous the fourth constant merely shifts the solution (2.6) in time. When (2.6) is valid, the trajectory is a space filling curve because the ratio of frequencies is irrational and occupies a rectangle of dimension $2a \times 2b$.

A nonlinear normal mode is defined here as the Hill–Poincaré analytical continuation of a linear normal mode into the nonlinear regime. A solution to (2.3) is $\varphi = d\varphi/dt = 0$ which means the in-plane libration can have a large amplitude without exciting the out-of-plane motion. In the orbital plane of the center of mass the libration of the gravity gradient pendulum is governed by

$$\frac{d^2\lambda}{dt^2} + \frac{3}{2}n^2 \sin 2\lambda = 0, \tag{2.7}$$

which is a simple pendulum equation (see Hughes, [2, pp. 298–301], for a discussion of its solution in the context of the gravity gradient pendulum). Such an equation is integrated by elliptic functions or equivalently by the analytical continuation of the solution (2.6b) by the Poincaré–Lindstedt method as shown in Melvin [12]. Thus the in-plane nonlinear normal mode is that of a half-angle simple pendulum.

Surfaces corresponding to different values of the constant C in (2.4) are the zero velocity curves which isolate the motion to reside within regions where the kinetic energy is positive. Set the time derivatives in (2.4) to zero to obtain

$$C^2 = \frac{1}{4}(1 + 3\cos^2\lambda)\cos^2\varphi. \tag{2.8}$$

Since the maximum value of C is unity for both time derivatives to be zero, it is possible to define

$$C = \cos\varphi_0, \tag{2.9}$$

where the value of φ_0 determines the zero velocity curve which passes through the latitudes $\varphi = \pm\varphi_0$ when $\lambda = 0$.

In Figure 1 the zero velocity curves from (2.8) are plotted for 5° increments in φ_0. The curves are plotted on the projection of a sphere on which is plotted a latitude-longitude grid in 45° increments. Points on the surface of this unit sphere represent directions from the center of mass of the gravity gradient pendulum. The locations of the equilibrium solutions are apparent from this figure. The nadir direction is stable and has the maximum, unit value of C. The along track direction is unstable with the value of $C = 1/2$. The orbit normal direction is also an unstable equilibrium with the value of zero for C.

A trajectory for a moderate amplitude, numerical solution of (2.3) is plotted in Figure 1. The initial conditions are $\varphi = 10°$, $\lambda = 20°$, $d\varphi/dt = d\lambda/dt = 0$. Although this solution is in the nonlinear regime, it shows the same qualitative behavior as (2.6). The solution is limited to a spherical rectangle centered on the nadir direction

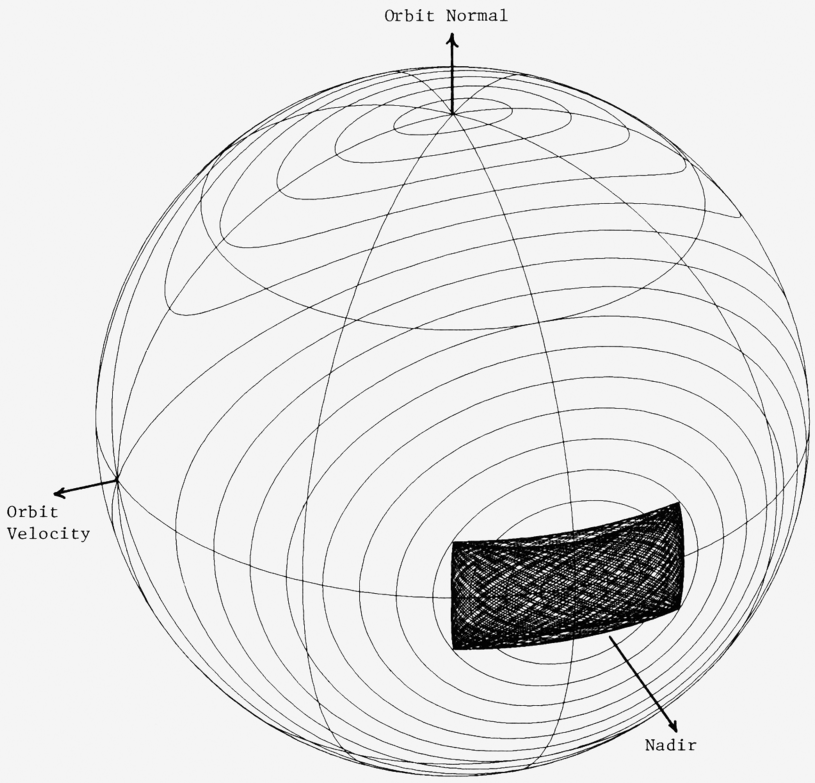

FIG. 1. A moderate amplitude libration of the gravity gradient pendulum

whose corners touch the zero velocity curve, and the trajectory apparently fills the rectangle. There are additional isolating integrals which keep the solution from filling the zero velocity curve. These integrals in the case of the linear solution (2.6) are the constants a and b. A nonlinear effect is visible in the trajectory in Figure 1. Since the two linear normal mode solutions of (2.6) are independent of each other, their trajectory would fill the rectangle uniformly. The ghost of curves interior to the bounding rectangle of Figure 1 indicate a nonlinear coupling between the modes.

Although it is always present, the gravity gradient torque is rather weak and easily overcome by other environmental forces. Hughes notes that for a passive system [2, p. 345], "It is apparently possible to directionally stabilize the vertical (two-axis stabilization) to within $\sim 20°$ at synchronous altitudes if symmetry is used." The amplitudes of Figure 1 are chosen to illustrate such residual librations.

2.2. *Motivation for the solution.* The small amplitude solutions (2.6), the solution to (2.7), and the first integral (2.4) are about all that is hitherto "known" about the gravity gradient pendulum. The main subject of this paper is the Hill–Poincaré analytical continuation of the out-of-plane normal mode (2.6a). Set b to zero in (2.6) and substitute (2.6a) into (2.5b) to obtain

$$\frac{d^2\lambda}{dt^2} + 3n^2\lambda = -2n^2a^2 \sin 4nt, \tag{2.10}$$

the inhomogeneous part of which is integrated as

$$\lambda = \frac{2}{13}a^2 \sin 4nt, \tag{2.11}$$

which means that the analytical continuation of the normal mode out of the orbital plane excites an in-plane libration which is 90° out of phase from the latitude libration.

From (2.6a) and (2.11) there are two in-plane oscillations for each one out-of-plane. With the phase relation between the two degrees of freedom this means that the trajectory described by the solution is a figure-of-8. Although there are more harmonics, this morphology persists at all amplitudes. A curiosity is that although a figure-of-8 has symmetries that apparently permit the trajectory to be traversed in either direction, in fact only one time evolution along the trajectory is possible. As viewed from the Earth the loop of the figure-of-8 above the orbit plane is traversed clockwise by the nadir end of the pendulum and below counterclockwise. This fact is apparent from examination of (2.5b), or (2.6a) and (2.11). The failure of time reversal invariance is due to the Coriolis force in the rotating reference frame.

Substitution of (2.11) and (2.6a) into the right-hand side of (2.5a) yields

$$\frac{d^2\varphi}{dt^2} + 4n^2\varphi = n^2a^3\left(-\frac{18}{13}\cos 2nt + \frac{2}{39}\cos 6nt\right), \tag{2.12}$$

which is in undamped resonance. Note from (2.5a) that the coupling from the in-plane libration and the pendulum term both contribute to the two terms on the right-hand side of (2.12). To cast out the secular term by the method of Lindstedt, a new independent variable is introduced:

$$\tau = 2n\omega t, \tag{2.13}$$

where the frequency is expanded in amplitude

$$\omega^2 = 1 + \omega_1 a^2. \tag{2.14}$$

Expand the solution to (2.12) in a Poincaré series

$$\varphi = a\cos\tau + a^3 Q(\tau). \tag{2.15}$$

Substitute (2.13), (2.14), and (2.15) into (2.12) to obtain

$$\frac{d^2Q}{d\tau^2} + Q = \left(\omega_1 - \frac{9}{26}\right)\cos\tau + \frac{1}{78}\cos 3\tau. \tag{2.16}$$

Eliminate the secular term by the choice

$$\omega_1 = \frac{9}{26} \tag{2.17}$$

and integrate (2.16) to obtain

$$Q = \frac{1}{624}(\cos\tau - \cos 3\tau). \tag{2.18}$$

The solution (2.18) to (2.16) is chosen to include a portion of the solution to the homogeneous part of (2.16) so that the expansion parameter a is the initial amplitude

of the out-of-plane angle. In Melvin [12] the solution to the homogeneous part is suppressed to simplify the algorithm which leads to the interpretation of a as the linear amplitude. In Melvin [19] both interpretations are explored, and it is found that the Poincaré–Lindstedt solution converges for slightly larger values of the expansion parameter if the linear amplitude interpretation is made. The initial amplitude is used here primarily because of convenience. For a while consideration was given to identifying the expansion parameter with the angle in (2.9) which is equivalent to the integral (2.4) until it was found that imaginary values of C result at large amplitudes, i.e., the hyperenergetic solutions. So far a difference in the numerical convergence has not been found for different interpretations of the expansion parameter for the figure-of-8 librations of the gravity gradient pendulum.

To order a^3 the Poincaré–Lindstedt method suggests the existence of a two degree of freedom periodic libration of the gravity gradient pendulum out of the orbit plane. Except perhaps for checking the low-order computer results, little is gained by proceeding by hand to the next or higher orders because the number of nonlinear terms increases quite rapidly. Except for handling large powers, the foregoing example illustrates all of the salient features of the Poincaré–Lindstedt method. At this point it is just as easy to proceed to develop the general algorithm by use of the notational tricks of Melvin [12] and [19].

3. An algorithm for the generation of the figure-of-8 libration. With $\tau = 2n\omega t$ the equations of motion (2.3) become

$$\omega^2\varphi'' + \frac{1}{4}[(1 + 2\omega\lambda')^2 + 3\cos^2\lambda]\sin\varphi\cos\varphi = 0, \tag{3.1a}$$

$$(\omega^2\lambda'' + \frac{3}{4}\sin\lambda\cos\lambda)\cos\varphi = \omega\varphi'(1 + 2\omega\lambda')\sin\varphi, \tag{3.1b}$$

where primes denote derivatives with respect to τ. The choice of the independent variable is made to eliminate dimensions, introduce the Lindstedt frequency, and obtain at very small amplitudes the period of the out-of-plane solution as 2π with $\omega = 1$.

To reduce complexity the computational algorithm is limited to recursion relations involving at most two sums. This is partially accomplished by the replacement of the equations of motion (3.1) by the equivalent system:

$$H = \omega\varphi'\eta\sin\varphi, \tag{3.2a}$$

$$G\cos\varphi = H, \tag{3.2b}$$

$$\omega^2\lambda'' + \frac{3}{8}\sin 2\lambda = G, \tag{3.2c}$$

$$\eta = 1 + 2\omega\lambda', \tag{3.2d}$$

$$F = \frac{1}{4}\left(\frac{3}{2} + \eta^2 + \frac{3}{2}\cos 2\lambda\right), \tag{3.2e}$$

$$\omega^2\varphi'' + \frac{1}{2}F\sin 2\varphi = 0. \tag{3.2f}$$

The solution to the system (3.2) is affected in terms of combined power and Fourier series which are called Poisson series by Deprit [20]. The series and coefficients are

defined in Table I. Because of the occurrence of the first derivatives in (3.1), the solution series (I.1) resemble those for the van der Pol equation found in Melvin [19], Deprit and Schmidt [21], or Dadfar, Geer, and Anderson [22]. These Coriolis terms add an interesting twist to the generation of the nonlinear normal mode which the author had not envisioned in his study of periodic variable stars. In spite of the occurrence of the imaginary unit in Table I, the series are made real by reflection relations given in the algorithm. The real forms of the solution (I.1) are

$$\varphi = 2\sum_{m=0}^{\infty} a^{2m+1} \sum_{j=0}^{m} \varphi_{m,j}^{(1)} \cos[(2j+1)\tau], \tag{3.3a}$$

$$\lambda = -2\sum_{m=1}^{\infty} a^{2m} \sum_{j=1}^{m} \lambda_{m,j}^{(1)} \sin(2j\tau), \tag{3.3b}$$

along with the Lindstedt frequency (I.10)

$$\omega = \sum_{m=0}^{\infty} a^{2m} \omega_m^{(1)}. \tag{3.3c}$$

These series are seen to be direct generalizations of the polynomials of the previous section. They can be a solution of (3.2) only if a consistent computational algorithm can be devised to generate the coefficients. To do this, additional series are defined in Table I.

TABLE I. Series Definitions and Coefficient Bounds $(i = \sqrt{-1})$

(I.1) $\varphi = \sum_{m=0}^{\infty} a^{2m+1} \sum_{j=-m-1}^{m} \varphi_{m,j}^{(1)} e^{i(2j+1)\tau}, \quad \lambda = i\sum_{m=1}^{\infty} a^{2m} \sum_{j=-m}^{m} \lambda_{m,j}^{(1)} e^{i2j\tau}$

(I.2) $\varphi' = i\sum_{m=0}^{\infty} a^{2m+1} \sum_{j=-m-1}^{m} (2j+1)\varphi_{m,j}^{(1)} e^{i(2j+1)\tau}, \quad \lambda' = -\sum_{m=1}^{\infty} a^{2m} \sum_{j=-m}^{m} 2j\lambda_{m,j}^{(1)} e^{i2j\tau}$

(I.3) $\omega\varphi' = i\sum_{m=0}^{\infty} a^{2m+1} \sum_{j=-m-1}^{m} \dot{\varphi}_{m,j} e^{i(2j+1)\tau},$

$\omega\lambda' = -\sum_{m=1}^{\infty} a^{2m} \sum_{j=-m}^{m} \left[2j \sum_{k=1}^{m} \omega_{m-k}^{(1)} \lambda_{k,j}^{(1)}\right] e^{i2j\tau}$

(I.4) $\varphi^{2n} = \sum_{m=n}^{\infty} a^{2m} \sum_{j=-m}^{m} \varphi_{m,j}^{(2n)} e^{i2j\tau}, \quad \lambda^{2n} = \sum_{m=2n}^{\infty} a^{2m} \sum_{j=-m}^{m} \lambda_{m,j}^{(2n)} e^{i2j\tau}$

(I.5) $\varphi^{2n+1} = \sum_{m=n}^{\infty} a^{2m+1} \sum_{j=-m-1}^{m} \varphi_{m,j}^{(2n+1)} e^{i(2j+1)\tau}, \quad \lambda^{2n+1} = i\sum_{m=2n+1}^{\infty} a^{2m} \sum_{j=-m}^{m} \lambda_{m,j}^{(2n+1)} e^{i2j\tau}$

(I.6) $\frac{1}{2}\sin 2\varphi = \sum_{n=0}^{\infty} A_n \varphi^{2n+1} = \sum_{m=0}^{\infty} a^{2m+1} \sum_{j=-m-1}^{m} F_{m,j}^{(2)} e^{i(2j+1)\tau}, \quad A_n = \frac{(-4)^n}{(2n+1)!}$

(I.7) $\cos 2\lambda = \sum_{n=0}^{\infty} B_n \lambda^{2n}, \quad B_n = \frac{(-4)^n}{(2n)!}$

(I.8) $\sin\varphi = \sum_{n=0}^{\infty} C_n \varphi^{2n+1} = \sum_{m=0}^{\infty} a^{2m+1} \sum_{j=-m-1}^{m} H_{m,j}^{(2)} e^{i(2j+1)\tau}, \quad C_n = \frac{(-1)^n}{(2n+1)!}$

(I.9) $\cos\varphi = \sum_{n=0}^{\infty} D_n \varphi^{2n} = \sum_{m=0}^{\infty} a^{2m} \sum_{j=-m}^{m} H_{m,j}^{(4)} e^{i2j\tau}, \quad D_n = \frac{(-1)^n}{(2n)!}$

(I.10) $\omega^n = \sum_{m=0}^{\infty} a^{2m} \omega_m^{(n)}, \quad n = 1, 2, \quad \eta^n = \sum_{m=0}^{\infty} a^{2m} \sum_{j=-m}^{m} \eta_{m,j}^{(n)} e^{i2j\tau}$

(I.11) $\omega\varphi'\eta = i\sum_{m=0}^{\infty} a^{2m+1} \sum_{j=-m-1}^{m} H_{m,j}^{(1)} e^{i(2j+1)\tau}, \quad H = i\sum_{m=1}^{\infty} a^{2m} \sum_{j=-m}^{m} H_{m,j}^{(3)} e^{i2j\tau}$

(I.12) $G = i\sum_{m=1}^{\infty} a^{2m} \sum_{j=-m}^{m} G_{m,j} e^{i2j\tau}, \quad F = \sum_{m=0}^{\infty} a^{2m} \sum_{j=-m}^{m} F_{m,j}^{(1)} e^{i2j\tau}$

Equations (I.2) display the derivatives of (I.1), and equations (I.3) define coefficients for the combination of the Lindstedt frequency with the derivatives which occur in (3.2a) and (3.2d). Powers of the solution occur in the power series expansions of the circular functions in (3.2). It is convenient to define both even and odd powers in (I.4) and (I.5). It is this simple notational trick of associating the power of the Poisson series with a superscript that is fundamental to the method of Melvin [12] in the solution of nonlinear differential equations.

In equations (I.6), (I.7), (I.8), and (I.9) coefficients are defined for the power series expansions of the circular functions which occur in (3.2). The evaluation of the algorithm on the CRAY was limited to the 50th order because of storage limitations which occur directly because of the circular function coefficients. Since the solution is valid only to the pole, it would be better to approximate the circular functions by low-order polynomials and to improve the storage further by limiting the number of harmonics. Should it be necessary to generate the figure-of-8 coefficients again, it would be better first to reformulate the equations of motion in a coordinate system that is nonsingular at the orbit normal and then to see if the Poincaré–Lindstedt solution continues over the pole.

To a certain extent the definitions of coefficients and their associations are arbitrary in the design of a computational algorithm. The chief criterion has been to limit the number of sums to two. To meet this criterion Poisson series coefficients are defined for (I.6), (I.8), and (I.9), but this step is not necessary for (I.7). Coefficients for two powers of the Lindstedt frequency ω and the parameter η (see (3.2d)) are defined in (I.10). In the first equation of (I.11), coefficients are defined for an intermediate term in the computation of (3.2a), and the coefficients of (3.2a) are defined in the second. The Poisson series coefficients for H, G, and F of (3.2) are defined in (I.11) and (I.12).

Except for a few $j = 0$ terms and some sequences in the powers of λ, the series definitions of Table I and summation bounds define the only nonzero terms. For example, since the linear normal mode (2.6a) is proportional to a, the nth power of the out-of-plane angle defined in the first equations of (I.4) and (I.5) are proportional to the nth power of a. Similarly the in-plane response amplitude (2.11) begins with the square of a, and the beginning sum index is adjusted accordingly in the second equations of (I.4) and (I.5). The establishment of the j limits of summation for the Fourier polynomials of the Poincaré expansions is accomplished by examination of the first few terms of the power relations (I.4) and (I.5) and the computational algorithm.

The gravity gradient pendulum is rather nice because the Poisson series (I.1) certainly are not the most general series that can be defined for the nonlinear normal modes of a fourth-order system. The limitations of the solution series (I.1) to even or odd powers of the expansion parameter and the Fourier polynomials to even and odd arguments greatly simplify the solution algorithm. What is especially pleasing is that the gravity gradient pendulum is an idealization which has engineering applications (there are literally hundreds of artificial satellites that are nadir pointing because of

the gravity gradient) not just a system that is "cooked up" to illustrate a point of nonlinear mathematics.

The system (3.2) is written in the order of solution used in the algorithm of Table II. To start the algorithm the following conditions are used for $m = 0$:

$$\varphi^{(1)}_{0,0} = \varphi^{(1)}_{0,-1} = \tfrac{1}{2}, \tag{3.4a}$$

$$\dot{\varphi}_{0,0} = -\dot{\varphi}_{0,-1} = H^{(1)}_{0,0} = -H^{(1)}_{0,-1} = H^{(2)}_{0,0} = H^{(2)}_{0,-1} = F^{(2)}_{0,0} = F^{(2)}_{0,-1} = \tfrac{1}{2}, \tag{3.4b}$$

$$\eta^{(1)}_{0,0} = \eta^{(2)}_{0,0} = \varphi^{(0)}_{0,0} = \lambda^{(0)}_{0,0} = \omega^{(1)}_0 = \omega^{(2)}_0 = F^{(1)}_{0,0} = 1, \tag{3.4c}$$

$$A_0 = B_0 = C_0 = D_0 = 1. \tag{3.4d}$$

There has been considerable evolution of compilers since the programs for Melvin [12] and [19] were written. To accommodate the limitations of FORTRAN 66, all arrays in those papers were adjusted to begin at 1, and the algorithms were devised to use only positive subscripts. FORTRAN 77, PASCAL, and ADA allow negative subscripts, and the algorithm of Table II is defined with this in mind. This single language feature greatly reduces the number of terms necessary in the definition of the algorithm. Sums such as those in (1) are carried out for nonnegative values of j, and then the value of the sum is assigned to the array elements for both the positive and negative subscripts.

TABLE II. Computational Algorithm $(m \geq 1,\ m \geq j \geq 0)$

(1) $H^{(3)}_{m,j} = -H^{(3)}_{m,-j} = \sum_{k=0}^{m-1} \sum_{l=-k-1}^{k} H^{(1)}_{m-k-1,j-l-1} H^{(2)}_{k,l}$

(2) $G_{m,j} = -G_{m,-j} = H^{(3)}_{m,j} - \sum_{k=1}^{m-1} \sum_{l=-k}^{k} G_{m-k,j-l} H^{(4)}_{k,l}$

(3) $A_m = -2A_{m-1}/(m(2m+1))$

(4) $\lambda^{(2n)}_{m,j} = \lambda^{(2n)}_{m,-j} = -\sum_{k=1}^{m-2n+1} \sum_{l=-k}^{k} \lambda^{(2n-1)}_{m-k,j-l} \lambda^{(1)}_{k,l}, \qquad m \geq 2n \geq 2$

(5) $\lambda^{(2n+1)}_{m,j} = -\lambda^{(2n+1)}_{m,-j} = \sum_{k=1}^{m-2n} \sum_{l=-k}^{k} \lambda^{(2n)}_{m-k,j-l} \lambda^{(1)}_{k,l}, \qquad m \geq 2n+1 \geq 3$

(6) $\lambda^{(1)}_{m,j} = -\lambda^{(1)}_{m,-j} = -\left[G_{m,j} + 4j^2 \sum_{k=1}^{m-1} \omega^{(2)}_{m-k} \lambda^{(1)}_{k,j} - \tfrac{3}{4} \sum_{n=1}^{(m-1)/2} A_n \lambda^{(2n+1)}_{m,j}\right] / \left(4j^2 - \tfrac{3}{4}\right)$

(7) $\eta^{(1)}_{m,j} = \eta^{(1)}_{m,-j} = -4j \sum_{k=1}^{m} \omega^{(1)}_{m-k} \lambda^{(1)}_{k,j}$

(8) $\eta^{(2)}_{m,j} = \eta^{(2)}_{m,-j} = \sum_{k=0}^{m} \sum_{l=-k}^{k} \eta^{(1)}_{m-k,j-l} \eta^{(1)}_{k,l}$

(9) $B_m = -2B_{m-1}/(m(2m-1))$

(10) $F^{(1)}_{m,j} = F^{(1)}_{m,-j} = \tfrac{1}{4}\left[\eta^{(2)}_{m,j} + \tfrac{3}{2} \sum_{n=1}^{m/2} B_n \lambda^{(2n)}_{m,j}\right]$

(11) $\varphi^{(2n)}_{m,j} = \varphi^{(2n)}_{m,-j} = \sum_{k=0}^{m-n} \sum_{l=-k-1}^{k} \varphi^{(2n-1)}_{m-k-1,j-l-1} \varphi^{(1)}_{k,l}, \qquad m \geq n \geq 1$

(12) $\varphi^{(2n+1)}_{m,j} = \varphi^{(2n+1)}_{m,-j-1} = \sum_{k=0}^{m-n} \sum_{l=-k-1}^{k} \varphi^{(2n)}_{m-k,j-l} \varphi^{(1)}_{k,l}, \qquad m \geq n \geq 1$

(13) $\varphi^{(1)}_{m,j} = \varphi^{(1)}_{m,-j-1} = \left[\sum_{n=1}^{m} A_n \varphi^{(2n+1)}_{m,j} + \sum_{k=0}^{m-1} \sum_{l=-k-1}^{k} F^{(1)}_{m-k,j-l} F^{(2)}_{k,l} - (2j+1)^2 \sum_{k=1}^{m-1} \omega^{(2)}_{m-k} \varphi^{(1)}_{k,j}\right] / (4j(j+1)), \qquad j \neq 0, -1$

$$(14)\quad \varphi^{(1)}_{m,0} = \varphi^{(1)}_{m,-1} = -\sum_{l=1}^{m} \varphi^{(1)}_{m,l}$$

$$(15)\quad \omega^{(2)}_{m} = 2\left[\sum_{n=1}^{m} A_n \varphi^{(2n+1)}_{m,0} + \sum_{k=0}^{m-1}\sum_{l=-k-1}^{k} F^{(1)}_{m-k,l} F^{(2)}_{k,l} - \sum_{k=1}^{m-1} \omega^{(2)}_{m-k}\varphi^{(1)}_{k,0}\right]$$

$$(16)\quad \omega^{(1)}_{m} = \tfrac{1}{2}\left[\omega^{(2)}_{m} - \sum_{k=1}^{m-1} \omega^{(1)}_{m-k}\omega^{(1)}_{k}\right]$$

$$(17)\quad F^{(2)}_{m,j} = F^{(2)}_{m,-j-1} = \sum_{n=0}^{m} A_n \varphi^{(2n+1)}_{m,j}$$

$$(18)\quad \dot{\varphi}_{m,j} = -\dot{\varphi}_{m,-j-1} = (2j+1)\sum_{k=0}^{m} \omega^{(1)}_{m-k}\varphi^{(1)}_{k,j}$$

$$(19)\quad H^{(1)}_{m,j} = -H^{(1)}_{m,-j-1} = \sum_{k=0}^{m}\sum_{l=-k}^{k} \dot{\varphi}_{m-k,j-l}\eta^{(1)}_{k,l}$$

$$(20)\quad C_m = -C_{m-1}/(2m(2m+1))$$

$$(21)\quad H^{(2)}_{m,j} = H^{(2)}_{m,-j-1} = \sum_{n=0}^{m} C_n \varphi^{(2n+1)}_{m,j}$$

$$(22)\quad D_m = -D_{m-1}/(2m(2m-1))$$

$$(23)\quad H^{(4)}_{m,j} = H^{(4)}_{m,-j} = \sum_{n=1}^{m} D_n \varphi^{(2n)}_{m,j}$$

From the values of conditions (3.4), the equations of Table II are computed by incrementing m. The first equation of Table II is the coefficient of H defined by (3.2a) and the second equation of (I.11). For $m = 1$ there is no contribution to H from ω or η, just the terms that lead to the right-hand side of (2.10). In programming (1) and the similar equations of Table II, it is necessary to check that the subscripts of the first term are within the bounds of definition of the coefficient. The limits on the k and l sums are established for nonzero values of the second term. An array element for the first term is not accessed unless $-m + k \leq j - l - 1 \leq m - k - 1$. These limits are established from the range in the sums of Table I, which in this case is the first equation of (I.11).

Equation (2) of Table II evaluates the coefficients of G defined in the first equation of (I.12) and (3.2b). In essence (2) is the way Poisson series are manipulated to multiply H by the secant of φ. For $m = 1$ the sum in (2) is not evaluated. For $m = 1$ equations (1) and (2) depend solely on conditions (3.4b). For $m > 1$ the terms that occur in (1) and (2) have been computed in (19), (21), and (23).

Equations (3), (9), (20), and (22) merely evaluate the coefficients of the power series of the circular functions defined in the last parts of equations (I.6), (I.7), (I.8), and (I.9).

Equations (4) and (5) compute the coefficients of powers of the in-plane response amplitudes. These recursion relations are derived by substitution of the second equations of (I.1), (I.4), and (I.5) into the identities

$$\lambda^{2n} = \lambda^{2n-1}\lambda, \qquad \lambda^{2n+1} = \lambda^{2n}\lambda.$$

Because they do not execute until $m \geq 3$, the most difficult problem in the derivation of Table II is the placement of the power relations (4) and (5).

The response amplitudes of (3.3b) are evaluated in equation (6), which is derived form (3.2c) by substitution of the appropriate series from Table I. The first term G in (6) is obtained directly from (I.12). The middle term of (6) comes from the

multiplication of the square of the Lindstedt frequency with the second derivative of (3.3b). The $k = m$ term of this sum gives the subscript of the coefficient on the left-hand side, and its contribution is the first portion of the divisor. The middle sum is nonzero only for $m > 1$. The last sum of (6) is derived by substitution of the second series of (I.5) into the first equation of (I.6). The $n = 0$ term of the last sum again produces the subscript of the left-hand side of (6) and is accounted for by the 3/4 in the divisor. The last sum of (6) is nonzero only for $m > 2$. The upper bound in the last sum means the integer value of the expression; for example, for $m = 3$ and $m = 4$, the upper bound is 1.

Equation (7) is derived from (3.2d) by substitution of the second equations of (I.10) and (I.3). Equation (8) is merely the square of η. The coefficient of the frequency modulation of the back couple (3.2e) is then computed in (10). Note that the constant terms of η and F which are unity are set in the conditions (3.4c). The power coefficients of φ are computed in (11) and (12) which are derived from the same identities as λ.

The out-of-plane amplitudes of (3.3a) and Lindstedt frequency coefficients (3.3c) of the nonlinear normal mode are computed in equations (13), (14), and (15). Since they are not obvious from (3.2f), their derivation is next explained. From the first equations of (I.1) and (I.10) and from the second equations of (I.6) and (I.12), one obtains

$$\omega^2\varphi'' = -\sum_{m=0}^{\infty} a^{2m+1} \sum_{j=-m-1}^{m} (2j+1)^2 e^{i(2j+1)\tau} \sum_{k=0}^{m} \omega_{m-k}^{(2)} \varphi_{k,j}^{(1)}, \tag{3.5}$$

$$\frac{1}{2} F \sin 2\varphi = \sum_{m=0}^{\infty} a^{2m+1} \sum_{j=-m-1}^{m} e^{i(2j+1)\tau} \sum_{k=0}^{m} \sum_{l=-k-1}^{k} F_{m-k,j-l}^{(1)} F_{k,l}^{(2)}. \tag{3.6}$$

Substitution of (3.5) and (3.6) into (3.2f) yields, upon equating like coefficients,

$$-(2j+1)^2 \sum_{k=0}^{m} \omega_{m-k}^{(2)} \varphi_{k,j}^{(1)} + \sum_{k=0}^{m} \sum_{l=-k-1}^{k} F_{m-k,j-l}^{(1)} F_{k,l}^{(2)} = 0. \tag{3.7}$$

Equation (17) is derived by substitution of the first equation of (I.5) into the first equation of (I.6). Break the first term out of (17) to obtain

$$F_{m,j}^{(2)} = \varphi_{m,j}^{(1)} + \sum_{n=1}^{m} A_n \varphi_{m,j}^{(2n+1)}. \tag{3.8}$$

In (3.7) extract the terms in the first sum at $k = 0$ and m and in the second sum at $k = m$ to obtain

$$-(2j+1)^2 \left[\omega_m^{(2)} \varphi_{0,j}^{(1)} + \omega_0^{(2)} \varphi_{m,j}^{(1)} + \sum_{k=1}^{m-1} \omega_{m-k}^{(2)} \varphi_{k,j}^{(1)} \right] + \sum_{l=-m-1}^{m} F_{0,j-l}^{(1)} F_{m,l}^{(2)} + \sum_{k=0}^{m-1} \sum_{l=-k-1}^{k} F_{m-k,j-l}^{(1)} F_{k,l}^{(2)} = 0. \tag{3.9}$$

Use (3.8), (3.4a), and (3.4c) and regroup to obtain

$$(2j+1)^2\omega_m^{(2)}\varphi_{0,j}^{(1)} + 4j(j+1)\varphi_{m,j}^{(1)} = \sum_{n=1}^{m} A_n\varphi_{m,j}^{(2n+1)} + \sum_{k=0}^{m-1}\sum_{l=-k-1}^{k} F_{m-k,j-l}^{(1)}F_{k,l}^{(2)} - (2j+1)^2\sum_{k=1}^{m-1}\omega_{m-k}^{(2)}\varphi_{k,j}^{(1)}. \quad (3.10)$$

With $j \neq 0, -1$ and conditions (3.4a), equation (3.10) gives (13); otherwise, it results in (15) where $\varphi_{m,0}^{(1)}$ is arbitrary. Evaluate (3.3a) at $\tau = 0$ to obtain by (3.4a) the initial value

$$\varphi(0) = a + 2\sum_{m=1}^{\infty} a^{2m+1}\sum_{j=0}^{m}\varphi_{m,j}^{(1)}.$$

If the expansion parameter a is identified with the initial value of φ, then the sum must be made to vanish by (14). To change the interpretation of the expansion parameter from the initial value to the linear amplitude, merely set the right-hand side of (14) to zero and eliminate the last sum of (15). The initial-value interpretation is far more convenient for plotting the solutions. For other initial conditions such as (4.3), the recursion relation (14) means that the expansion parameter is the maximum latitude.

Equation (16) of Table II extracts the square root of the power series representing the square of the Lindstedt frequency which is computed in (15). Equation (17) is examined in (3.8) and represents the computation of the Poisson series coefficients of the sine of the out-of-plane angle. It must be computed after the update of the latitude coefficients in (13) and (14). The coefficients of the first equation of (I.3) are computed in (18). The dot in this coefficient does not represent a time derivative but rather the coefficient in the series of the time derivative of the latitude. This coefficient is explicitly defined to limit the number of sums in (19) to two.

Equation (19) of Table II is for the computation of the coefficients defined in the second equation of (I.11) of the Poisson series expansion of the parameter H defined in (3.2a). The parameter H is velocity dependent and determines the in-plane coupling of the out-of-plane motion. Equations (21) and (23) compute the Poisson series coefficients in the circular function expansions (I.8) and (I.9).

4. Numerical results. The algorithm of Table II is coded in FORTRAN 77 and was executed in double precision on a CRAY XMP to order $m = 50$. Beyond about this order the CRAY no longer has sufficient memory to contain the arrays. Perhaps a higher order may be achieved by limitation of the number of harmonics and power coefficients. The results of this execution are summarized in Figures 2 and 3 and Table III. The solution coefficients are used in (3.3a) and (3.3b) to generate values which are in turn plotted to give the trajectories in Figure 2. The initial value of the out-of-plane latitude a is in 5° increments for the plots in the range from 5° to 90°.

The essence of the method of Lindstedt is the dependence of the solution frequency or period on amplitude. In Figure 3 the frequencies and periods are plotted for both normal modes of the gravity gradient pendulum. The dimensionless curves are

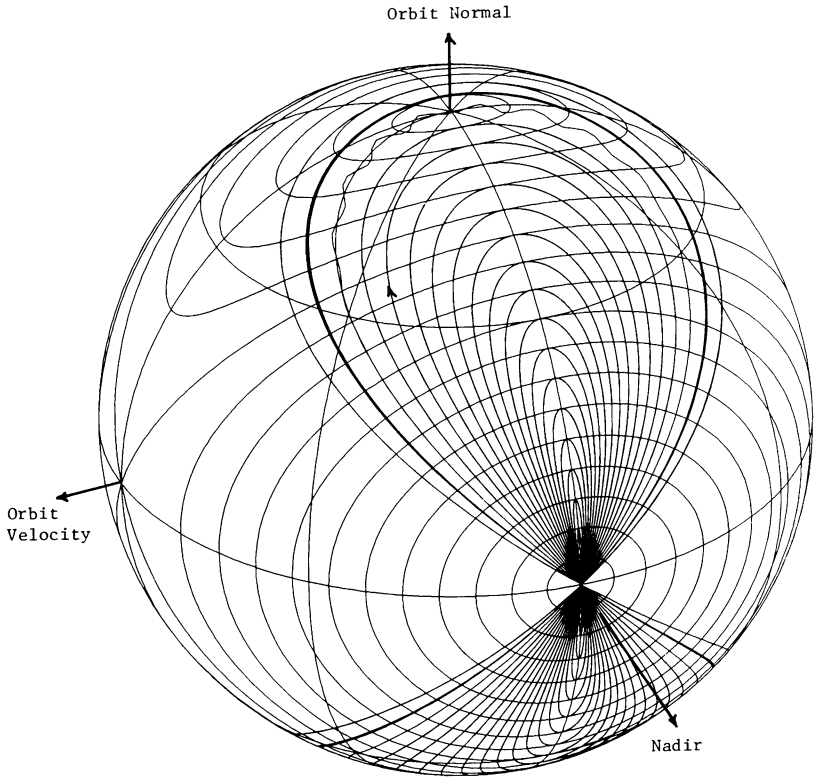

FIG. 2. Trajectories of the figure-of-8 libration of the gravity gradient pendulum

generated from the 29th and 30th order polynomials for the in-plane and 49th and 50th order for the out-of-plane. The plots are normalized to the orbital frequency n or the orbital period $2\pi/n$. This means that given an orbital period of say 100 minutes the corresponding gravity gradient pendulum periods at a given amplitude can be obtained by multiplication of the specific orbit frequency or period by the value in the figure. For comparison, a plot of the in-plane normal mode spectrum is given in Hughes [2, Fig. 9.8, p. 300].

The curve marked by 1 in Figure 3 is the frequency of the normal mode in the orbital plane of the center of mass obtained by generation of the solution to (2.7) to order 30. The curve marked by 2 is the reciprocal of this frequency which is the period of the oscillation per orbit period. The curve marked by 3 is the frequency of the figure-of-8 libration (3.3c). Its reciprocal is the libration period per orbit period and is marked by 4. The orbit frequency for the in-plane normal mode reaches unity (one oscillation per orbit) at an amplitude of about 74°, and the figure-of-8 reaches unity at an amplitude of about 104°. In Table III the first column of double precision numbers are the coefficients for (3.3c) as obtained from the CRAY truncated to 16 places.

TABLE III. Frequency and Initial Condition Coefficients

m	$\omega_m^{(1)}$	$\dot{\varphi}_m(0)$	$\dot{\lambda}_m(0)$
1	$-1.7307692307692308D-01$	$-1.28205128205128 21D-02$	$-6.1538461538461538D-01$
2	$1.3078914428766500D-02$	$3.9865107287383939D-02$	$-1.5734819711927094D-01$
3	$-5.3002923561582954D-04$	$1.0725699030262359D-02$	$-9.7806004349132618D-03$
4	$-2.1761757737079484D-04$	$1.5957470843836395D-04$	$4.4543213933400251D-03$
5	$-4.0991485807365618D-05$	$-5.3520163456592312D-04$	$1.0588285466712442D-03$
6	$-5.6388557127406506D-07$	$-9.6712045404416939D-05$	$-1.0330135685786282D-04$
7	$8.0562572573344270D-07$	$1.6012697387394559D-05$	$-8.4170160352781359D-05$
8	$-1.3603821616200824D-07$	$8.2650780171046832D-06$	$-8.7255545081095884D-06$
9	$-1.2877535568718548D-07$	$1.9579054600673957D-07$	$3.3335510523163532D-06$
10	$-2.4352706329386168D-08$	$-5.1583107118253700D-07$	$8.9726807684803366D-07$
11	$1.0350758150116530D-09$	$-8.9412625087349246D-08$	$-1.2601895971525997D-07$
12	$7.6309173355995386D-10$	$2.2140492495793065D-08$	$-8.7763904590085329D-08$
13	$-2.0906609584992558D-10$	$9.3812847675353594D-09$	$-6.1964684447995349D-09$
14	$-1.4233351549172771D-10$	$-2.4295199144111982D-10$	$4.6982283217386783D-09$
15	$-2.0598317424642045D-11$	$-7.1991883967820910D-10$	$9.6797153452939654D-10$
16	$3.2503350401993806D-12$	$-8.8441034832482439D-11$	$-2.4039158775113088D-10$
17	$8.9929772981123744D-13$	$3.9958938423141674D-11$	$-1.1597341651140712D-10$
18	$-3.8122586225818162D-13$	$1.2290440055160658D-11$	$-1.5972427548071899D-12$
19	$-1.9026884346796582D-13$	$-1.2597671215790673D-12$	$7.7622832108971568D-12$
20	$-1.6802770977435036D-14$	$-1.1276264762962433D-12$	$1.0647135367669240D-12$
21	$7.1137388504410160D-15$	$-7.0743365356803386D-14$	$-4.8470217202740929D-13$
22	$1.0158690784882793D-15$	$7.5879786747424645D-14$	$-1.6507818531587557D-13$
23	$-7.3464327890245664D-16$	$1.6407165214834844D-14$	$9.9368185752765195D-15$
24	$-2.7245845609879540D-16$	$-3.5614775577681988D-15$	$1.3369894061623000D-14$
25	$-5.9522615993117533D-18$	$-1.8220916648118699D-15$	$9.4139838682798312D-16$
26	$1.4043993634530636D-17$	$8.8881559927950573D-18$	$-9.7498890490084065D-16$
27	$8.1192151125028796D-19$	$1.4435798265269186D-16$	$-2.3446496848113095D-16$
28	$-1.4359655546231300D-18$	$2.0285035917289033D-17$	$3.8100211058588891D-17$
29	$-3.9294648253245525D-19$	$-8.5838157962436194D-18$	$2.2999965273355806D-17$
30	$2.4314367086129402D-20$	$-2.9087625221118708D-18$	$1.8392143950683654D-20$
31	$2.6096819474378179D-20$	$2.5322901044176328D-19$	$-1.9269477262989567D-18$
32	$-4.7638946542181860D-22$	$2.6996327042190917D-19$	$-3.1010916229166857D-19$
33	$-2.7914052581950725D-21$	$1.9126450485514089D-20$	$1.0277460091981069D-19$
34	$-5.4092186587450573D-22$	$-1.9114174699359529D-20$	$3.8475315849649081D-20$
35	$9.9455611236916634D-23$	$-4.4151763315019125D-21$	$-3.0990356510380072D-21$
36	$4.5802511489730002D-23$	$8.9038719337968817D-22$	$-3.7106093218794114D-21$
37	$-4.7090640432690194D-24$	$4.8969338363143329D-22$	$-3.3341858620835636D-22$
38	$-5.3301110708293654D-24$	$-5.3292052771335831D-25$	$2.4342993332221350D-22$
39	$-6.5159943372801031D-25$	$-4.0307966762247941D-23$	$6.0802450007711957D-23$
40	$2.7070892698891356D-25$	$-6.0005305499669684D-24$	$-1.1591196396536301D-23$
41	$7.4749208459558263D-26$	$2.4038510446114212D-24$	$-6.9025817446287741D-24$
42	$-1.6146539744584737D-26$	$8.4835225998818159D-25$	$-1.2775295998211715D-25$
43	$-9.8910574763784910D-27$	$-7.2520545181794710D-26$	$5.3468355937907211D-25$
44	$-5.1176182470458294D-28$	$-8.1087125599541152D-26$	$8.6318313382827619D-26$
45	$6.3617194516024559D-28$	$-6.1803689978621465D-27$	$-3.2334768579684260D-26$
46	$1.0863655367532828D-28$	$5.7691072319763533D-27$	$-1.2253741967703350D-26$
47	$-4.4035651468180413D-29$	$1.3689543995725268D-27$	$7.6773066109181712D-28$
48	$-1.7612816954735681D-29$	$-2.7561028595496868D-28$	$1.1087669809971149D-27$
49	$4.5665243442645583D-31$	$-1.5538498914903989D-28$	$9.5991540673313341D-29$
50	$1.3717685050130240D-30$	$-4.3164244814460687D-31$	$-7.9452593102334946D-29$

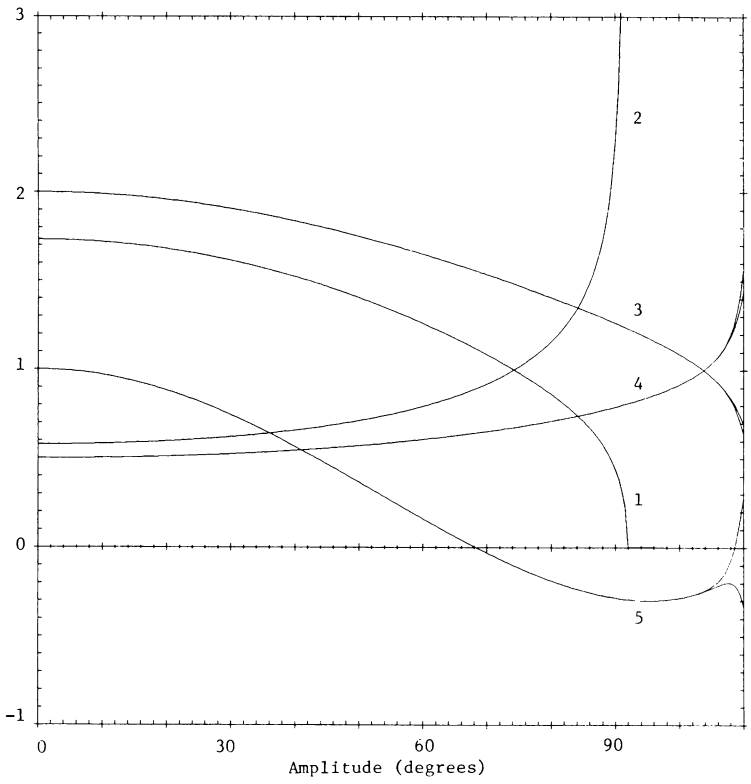

FIG. 3. The dynamical spectrum of the gravity gradient pendulum

During the generation of the numerical solutions, it was noticed that the value of the constant C in the first integral becomes imaginary for amplitudes greater than about 68°. It is found numerically that the algebraic function (2.4) is indeed constant, but the kinetic energy term which is set to zero to obtain (2.8) becomes large enough that the value of the left-hand side of (2.4) is positive. These large amplitude solutions are called *hyperenergetic*. The curve marked with 5 in Figure 3 is a plot of the values of C^2 at orders 49 and 50. On the issue of the continuation of the Poincaré–Lindstedt solution over the pole, note from curves 3, 4, and 5 that judged by the behavior of the 49th and 50th order polynomials the series converge well beyond the orbit normal.

It is not clear what these hyperenergetic solutions mean. For one thing the motion can never come to rest because the zero velocity curves do not exist, but the figure-of-8 libration has this property for all nonzero amplitudes. Most intuition about potential motion is based on systems either with or reducible to one degree of freedom. In such systems hyperenergetic solutions cannot exist in a bound state. Yet for the gravity gradient pendulum, bound, two-dimensional motions exist even though the energy is more than sufficient for unbounded motions. It is as if a baseball were to be thrown over an ordinary water well, and it then proceeds to bounce back and forth over the top of the well without touching anything. One wonders if it is possible to store and extract this libration energy for other purposes such as orbit modification.

4.1. *Coefficients as rational fractions.* It is apparent from the motivation for the solution of Section 2.2 that the coefficients of the solution (3.3) are rational fractions. To proceed to very high orders it is necessary to use floating point representations for the coefficient arrays defined in Table I, but such approximations lack the elegance of the rational fraction approximations found in Dasenbrock [13], Deprit and Schmidt [21], or Dadfar, et al. [22]. In collaboration with V. A. Brumberg, Dasenbrock has developed FORTRAN subroutines for the addition and multiplication of rational fractions based on the Euclidean factorization algorithm. The program for Table II was modified to purely integer arrays for numerators and denominators and Dasenbrock's subroutines incorporated. The results depend on the integer word length for a given computer. With 64 bit integers on the CRAY the $m = 4$th and part of the 5th order solution is achieved. The resulting approximations to (3.3) are:

$$\varphi = a\cos\tau + a^3\left(\frac{1}{624}\cos\tau - \frac{1}{624}\cos 3\tau\right) \tag{4.1a}$$
$$+ a^5\left(-\frac{4,132,951}{514,625,280}\cos\tau + \frac{167,435}{25,731,264}\cos 3\tau + \frac{20,109}{13,195,520}\cos 5\tau\right)$$
$$+ a^7\left(-\frac{260,080,255,581,311}{83,780,855,605,923,840}\cos\tau + \frac{266,956,157,747}{127,326,528,276,480}\cos 3\tau\right.$$
$$\left. + \frac{4,724,813,373}{5,144,826,349,568}\cos 5\tau + \frac{248,449}{2,960,642,048}\cos 7\tau\right) + \cdots,$$

$$\lambda = \frac{2}{13}a^2\sin 2\tau + a^4\left(\frac{851}{13,182}\sin 2\tau + \frac{10}{793}\sin 4\tau\right) \tag{4.1b}$$
$$+ a^6\left(\frac{2,073,771,137}{130,457,508,480}\sin 2\tau + \frac{425,591}{49,050,222}\sin 4\tau + \frac{3,146,201}{2,418,738,816}\sin 6\tau\right)$$
$$+ a^8\left(\frac{4,726,851,923,422,897}{1,769,870,574,675,141,120}\sin 2\tau + \frac{454,780,528,077}{126,751,790,475,232}\sin 4\tau\right.$$
$$\left. + \frac{6,260,606,370,335}{4,687,738,349,379,072}\sin 6\tau + \frac{7,840,175}{50,995,076,704}\sin 8\tau\right) + \cdots,$$

$$\omega = 1 - \frac{9}{52}a^2 + \frac{1,839}{140,608}a^4 - \frac{15,365,843}{28,990,557,440}a^6 + \cdots. \tag{4.1c}$$

It is far easier to integrate the equations of motion (2.3) numerically than to produce analytical solutions. The initial conditions that will generate motions close to the figure-of-8 libration are obtained from (4.1) as

$$\varphi(0) = a, \qquad \dot{\varphi}(0) = \lambda(0) = 0, \tag{4.2a}$$

$$\dot{\lambda}(0) = 2n\omega\lambda'(0) = n\omega\sum_{m=1}^{\infty} a^{2m}\sum_{j=1}^{m}(-8j\lambda_{m,j}^{(1)}) \tag{4.2b}$$
$$= n\omega\left(\frac{8}{13}a^2 + \frac{144,382}{402,051}a^4 + \frac{3,473,885,326,411}{23,376,354,800,760}a^6\right.$$
$$\left. - \frac{345,885,674,321,761,167}{403,955,119,965,339,296}a^8 + \cdots\right).$$

It would be difficult in practice to maneuver a satellite to achieve the initial conditions (4.2).

To get a satellite actually to perform the figure-of-8 libration, it would be better first to stabilize to nadir pointing and then to impart an impulse which approximates the initial conditions

$$\varphi(0) = \lambda(0) = 0, \tag{4.3a}$$

$$\dot{\varphi}(0) = n\omega \sum_{m=0}^{\infty} a^{2m+1} \dot{\varphi}_m(0) \tag{4.3b}$$

$$= n\omega \left(-2a - \frac{1}{78}a^3 + \frac{2,564,449}{64,328,160}a^5 + \frac{597,478,884,127}{55,705,356,120,960}a^7 + \cdots \right),$$

$$\dot{\lambda}(0) = n\omega \sum_{m=1}^{\infty} a^{2m} \dot{\lambda}_m(0) \tag{4.3c}$$

$$= n\omega \left(-\frac{8}{13}a^2 - \frac{63,262}{402,051}a^4 - \frac{228,634,785,931}{23,376,354,800,760}a^6 + \cdots \right),$$

where

$$\dot{\varphi}_m(0) \equiv \sum_{j=0}^{m} (-1)^{j+1} 4(2j+1)\varphi_{m,j}^{(1)}, \tag{4.4a}$$

$$\dot{\lambda}_m(0) \equiv \sum_{j=1}^{m} (-1)^{j+1} 8j\lambda_{m,j}^{(1)}. \tag{4.4b}$$

The fact that these initial conditions are derived for $\tau = \pi/2$ instead of 0 is irrelevant because (2.3) is autonomous.

The initial conditions (4.3) give better results than (4.2) in the sense that there is less broadening of the trajectory from the figure-of-8. The conditions (4.3) are used to integrate the equations of motion (2.3) numerically, and the resulting trajectories are plotted in Figure 2. The derivation and programming of the algorithm of Table II is difficult, and an independent check is necessary. The easiest check is the numerical integration of (2.3) using fourth-order Runge-Kutta. The verification of Table II and its program are the results presented in Figure 2. Each trajectory up to 90° amplitude is actually a plot of both the numerical and the 50th order polynomial trajectories. For amplitudes to 85° the lack of doubling or broadening of the curves indicates the agreement of the numerical integration and polynomial evaluation to graphical accuracy, i.e., the plots of the two solutions are within the thickness of the plotter line.

4.2. *Over-the-pole solutions.* Most of this kind of study is in the gray area of applied mathematics. Although the analysis of Section 2.2 suggests the existence of the nonlinear normal mode out of the orbital plane, it does not predict the amplitudes where the solution exists. There are no means to determine beforehand the convergence of the series, and numerical results can only suggest when the series may converge. Upon first performing the analysis of Section 2.2, it was expected that the figure-of-8 solution would exist perhaps to amplitudes between 30° and 60°, say to

where the solution becomes hyperenergetic. The longitude series (3.3b) cannot converge to amplitudes greater than 90° because the form of the solution changes from oscillatory to circulatory. Thus it is rewarding that the solutions generated from Table II are apparently convergent almost to the orbit normal.

A proper stability analysis of the figure-of-8 libration requires an expansion in a small perturbation about the motion and an examination of its characteristic exponents. Such analysis is beyond the scope of this preliminary examination. In the meanwhile one must be satisfied with a few numerical experiments that give some indication of the phenomena involved.

Up to the orbit normal the out-of-plane nonlinear normal mode appears to be stable even in hyperenergetic cases. In Figure 4 there is a plot of a trajectory which results from a numerical integraton of initial conditions near an hyperenergetic nonlinear normal mode. That the integration remains near a figure-of-8 means either that the solution is stable or that the growth of the instability is very slow. A very large amplitude case is shown in Figure 4 where the maximum latitude is 85°. While debugging the computer program many other integrations at intermediate amplitudes were carried out with no indications of instability for initial conditions near the nonlinear normal mode except for the over-the-pole cases.

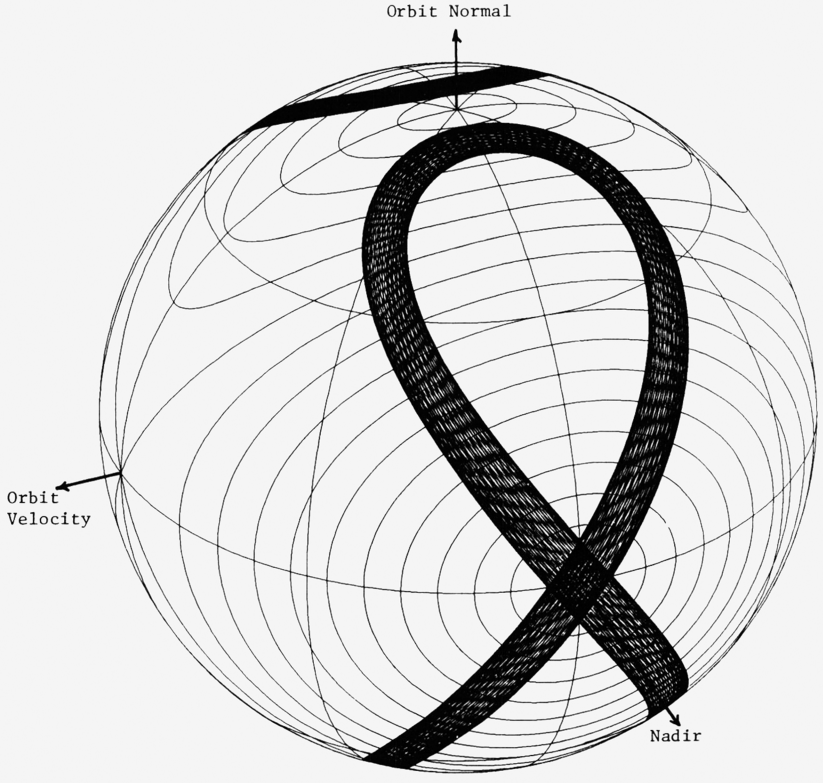

FIG. 4. A numerical integration illustrating the stability of the figure-of-8 libration

The solutions were initially plotted in a rectangular projection, but the spherical projection used in the figures has the advantage that it suggests the continuation of the hourglass solution beyond the orbit normal. In the neighborhood of the nadir direction the bundle of trajectories emanating from the origin appear to be well behaved. The problems with the polynomial trajectories begin appearing only near the pole (which is another reason not to use (4.2) as initial conditions). In the numerical integrator the initial conditions (4.3) are obtained from the coefficients (4.4) which are listed in Table III to order $M = 50$, and it is merely a matter of extending loop bounds to obtain initial conditions for amplitudes greater than 90°.

Recognizable figures-of-8 are found to amplitudes of 105°. The over-the-pole solutions appear to be unstable. In Figure 2 are plotted two figures-of-8 computed by numerical integration at amplitudes of 95° and 100°. The curve at 95° circulates several times, and the broadening of the curve is an indication of the instability. The 100° curve is only a few turns as it quickly leaves the figure-of-8 and wanders about the sphere.

Difficulties arise with the trajectories through the pole. The polynomial trajectory at $a = 90°$ shows secondary oscillations, and the numerical trajectory begins at the origin and terminates at the pole. Several attempts were made to complete the figure-of-8 through the pole which included trying to trace the other branch backwards from the origin to the pole (the failure of time reversal invariance becomes immediately apparent), but the Runge-Kutta integration would not proceed through the pole. It is hoped that the issues of the stability of the figures-of-8, the behavior at the orbit normal, and the relation to the three-body integrations of Bray and Goudas [15] will be part of a future study.

4.3. *Chaotic solutions.* To make sure that some other type of regular nonlinear motion does not exist, a series of numerical integrations were carried out. Besides finding some well-behaved solutions, it is apparent that there are large amplitude, pathological solutions to the gravity gradient pendulum equations. The trajectory for such a solution is displayed in Figure 5 and is generated from the initial conditions $\lambda = 60°$, $d\varphi/dt = d\lambda/dt = 0$. The initial value of φ is then determined from (2.8) with the value of $\varphi_0 = 60°$ in (2.9). Whether or not such solutions satisfy the presently accepted definition of chaotic solutions in terms of strange attractors, they certainly are in a different class from those shown in the other figures.

The most startling aspect of the solution in Figure 5 is the apparent filling of the zero velocity surface. Perhaps the small lunes at the top and bottom are not filled (the numerical integration proceeded to $nt = 1000$), but enough of it is filled that the chaotic behavior is apparent. These solutions are found by choosing initial conditions along the zero velocity curve for $C = 1/2$. For initial longitudes less than about 47.5° the motion is limited to regions smaller than the zero velocity curves. For greater longitudes the pathological solutions are found. For values of C less than $1/2$ the numerical solutions quickly begin tumbling in longitude, and their motion is not followed. For values of C slightly more than $1/2$ chaotic solutions are found. No attempt has been made to define more precisely the conditions under which well-behaved solutions like those of Figure 1 change into those similar to Figure 5.

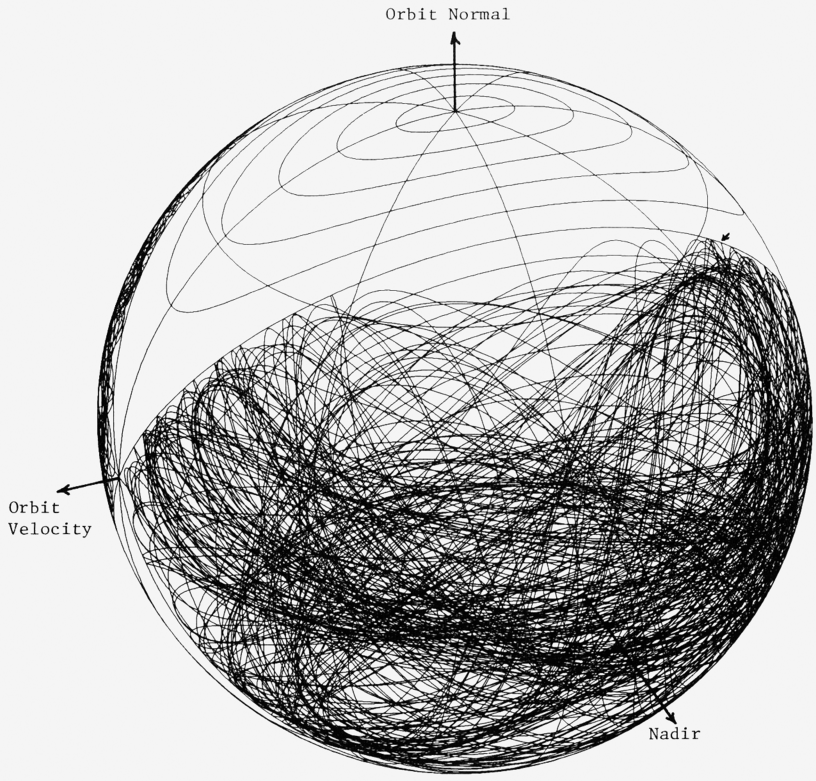

FIG. 5. A chaotic libration of the gravity gradient pendulum

Because the chaotic solutions are found so close to the zero velocity curve which restricts motion to a single hemisphere, it is unlikely that such motions could be achieved in practice without neglected perturbations causing the pendulum to begin tumbling in longtitude.

5. A theory of a tethered satellite. The gravity gradient pendulum is the simplest example of a tethered satellite and forms the basis for the analysis of orbit-tether interactions in Breakwell and Gearhart [23]. In such analyses one must wonder about the flexibility of the supposably rigid, massless rod which constitutes the tether. Such difficult questions will be addressed in later analyses, but first a simple analytical approach is devised for an N-element tether constructed out of $N + 1$ point masses where only the gravity gradient force is taken into account. The analytical solution is presented for a rosary tether where all lengths and masses are equal.

Consider $N + 1$ interacting particles moving in an inverse square law gravitational field. Assume that the forces of interaction satisfy Newton's third law, act along the line joining the neighboring particles, and only adjoining particles directly affect one another. Because the ith particle is affected only by the $(i - 1)$st and $(i + 1)$st, the tether problem differs from the N-body problem where each particle affects every other particle. The distance of the center of mass of the particles from the center of the Earth is assumed to be much larger than the length of the tether. Then it can be

shown that the center of mass moves in a Keplerian orbit which is further restricted to be circular.

With these hypotheses it is easily shown that the displacement of each particle from the next satisfies N coupled Hill equations of the form (2.1). The component equations of motion are of the same form as (2.2) except there are now force terms on the right-hand sides of the angular equations. The system is next assumed to be near its stable equilibrium which points at the center of the Earth, and the equations of motion are linearized.

The assumption that each segment is of constant length supplies N constraint equations in N unknown forces for the radial components as

$$-\frac{1}{m_{i-1}}F_{i-2,i-1}+\left(\frac{1}{m_{i-1}}+\frac{1}{m_i}\right)F_{i-1,i}-\frac{1}{m_i}F_{i,i+1}=3n^2\rho_i, \qquad i=1,\ldots,N, \quad (5.1)$$

where m_i is the mass of the ith particle, where $F_{i-1,i}$ is the magnitude of the force of the ith particle on the $(i-1)$st (assumed to be zero for subscripts which are negative or greater than N), and where ρ_i is the distance between the $(i-1)$st and ith particle. Because equations (5.1) are determinable, the magnitude of the forces between the particles that form the tether have been completely specified by constraining the tether segments to be of constant length.

The motions in- and out-of-plane uncouple in the linear regime, and the angular equations of motion are

$$\frac{d^2}{dt^2}\varphi_i+4n^2\varphi_i=\frac{1}{\rho_i m_{i-1}}F_{i-2,i-1}(\varphi_{i-1}-\varphi_i)+\frac{1}{\rho_i m_i}F_{i,i+1}(\varphi_{i+1}-\varphi_i), \quad (5.2a)$$

$$\frac{d^2}{dt^2}\lambda_i+3n^2\lambda_i=\frac{1}{\rho_i m_{i-1}}F_{i-2,i-1}(\lambda_{i-1}-\lambda_i)+\frac{1}{\rho_i m_i}F_{i,i+1}(\lambda_{i+1}-\lambda_i), \quad (5.2b)$$

where φ_i and λ_i are the latitude and longitude of the ith tether segment measured at the center of mass. The equations of motion (5.2) can be solved once the forces of constraint are obtained from the solution of (5.1). Interestingly the coupling is of the same form on the right-hand sides of (5.2a) and (5.2b). Note from (5.2) and (5.4) that independent of the mass distribution there are the solutions in which all of the in-plane or out-of-plane angles are equal. This means that the gravity gradient pendulum is the fundamental mode of any tethered satellite.

The linearized equations of motion are homogeneous systems which means the solutions are determined by eigenvalue problems; that is, the general solution to (5.2) is

$$\varphi_i=\sum_{j=1}^{N}\varphi_{i,j}[a_j\cos(\omega_j nt)+b_j\sin(\omega_j nt)], \quad (5.3a)$$

$$\lambda_i=\sum_{j=1}^{N}\lambda_{i,j}[c_j\cos(\nu_j nt)+d_j\sin(\nu_j nt)], \quad (5.3b)$$

where a_j, b_j, c_j, and d_j are sequences of arbitrary constants, ω_j and ν_j are the out-of- and in-plane eigenvalues, and $\varphi_{i,j}$ and $\lambda_{i,j}$ are the eigenvectors associated with the eigenvalues.

Substitution of (5.3) into (5.2) yields the eliminants

$$\frac{1}{\rho_i m_{i-1}} F_{i-2,i-1}\varphi_{i-1,j} + \left(n^2\omega_j^2 - 4n^2 - \frac{1}{\rho_i m_{i-1}} F_{i-2,i-1} - \frac{1}{\rho_i m_i} F_{i,i+1}\right)\varphi_{i,j} + \frac{1}{\rho_i m_i} F_{i,i+1}\varphi_{i+1,j} = 0, \quad (5.4a)$$

$$\frac{1}{\rho_i m_{i-1}} F_{i-2,i-1}\lambda_{i-1,j} + \left(n^2\nu_j^2 - 3n^2 - \frac{1}{\rho_i m_{i-1}} F_{i-2,i-1} - \frac{1}{\rho_i m_i} F_{i,i+1}\right)\lambda_{i,j} + \frac{1}{\rho_i m_i} F_{i,i+1}\lambda_{i+1,j} = 0. \quad (5.4b)$$

Thus, given the masses and segment lengths, the problem of the description of the motion of a tethered satellite has been reduced in the linear regime to two algebraic problems. First the system (5.1) is solved for the forces of constraint. Second the eigenvalue problems (5.4) are solved again in two steps. First the eigenvalues are found as the roots of the characteristic equation which is found by setting the determinants of the coefficients in (5.4) equal to zero. Second the eigenvectors are generated from (5.4).

What is especially appealing about the above approach is that it has not been necessary to go beyond the concepts of particle dynamics to obtain a complete description of the motion of an orbiting tether. That is, it has been necessary neither to derive partial differential equations with their attendant, mysterious boundary conditions nor to consider the material that makes up the tether other than the general hypothesis that it be strong enough to supply the forces of constraint. For this preliminary analysis it is also assumed that the tether has no restoring or frictional forces. Because of the multiple segment approach, it is possible to examine both tether models which are composed of rigid rods and the transition to the continuous case of a large number of segments.

The eigenvalues and vectors are dependent on the tether model, and their production can be a difficult operation requiring very specialized software. There is, however, one tether model that can be solved. The *rosary tether* is defined to be made up of equal masses and equal length segments:

$$m_i = m, \qquad \rho_i = \rho. \quad (5.5)$$

The equations of constraint (5.1) are then

$$-F_{i-2,i-1} + 2F_{i-1,i} - F_{i,i+1} = 3mn^2\rho. \quad (5.6)$$

Eric Mokole of the Naval Research Laboratory has provided the solution to this finite difference equation as

$$F_{i-1,i} = \frac{3}{2} mn^2\rho(N - i + 1)i, \quad (5.7)$$

which may be verified by direct substitution.

The eliminants for the rosary tether are obtained by substitution of the rosary conditions (5.5) and the forces of constraint (5.7) into (5.4):

$$\frac{3}{2}(N-i+2)(i-1)\varphi_{i-1,j}+\{\omega_j^2-4+3[i^2-i(N+1)+1]\}\varphi_{i,j}+\frac{3}{2}(N-i)(i+1)\varphi_{i+1,j}=0, \quad (5.8a)$$

$$\frac{3}{2}(N-i+2)(i-1)\lambda_{i-1,j}+\{\nu_j^2-3+3[i^2-i(N+1)+1]\}\lambda_{i,j}+\frac{3}{2}(N-i)(i+1)\lambda_{i+1,j}=0. \quad (5.8b)$$

By consideration of the roots of the characteristic equation sequentially up to $N = 5$ and by numerical verification to very high orders, the eigenvalues of (5.8) have been found to be

$$\omega_j^2 = 4+\frac{3}{2}(j-1)(j+2), \qquad \nu_j^2 = 3+\frac{3}{2}(j-1)(j+2). \quad (5.9)$$

A curiosity of the eliminants (5.8) is that the roots of the characteristic equation (5.9) are independent of N, i.e., the roots for N are also roots of the characteristic equation for $N+1$. The eigenvectors, however, differ for each value of N.

Substitution of (5.9) into (5.8) gives the same eliminant for both coordinates as

$$(N-i+2)(i-1)\varphi_{i-1,j}+[2i(i-1-N)+j(j+1)]\varphi_{i,j}+(N-i)(i+1)\varphi_{i+1,j}=0. \quad (5.10)$$

The most difficult task of the determination of the eigenvalues is complete for the rosary tether. It is next merely a matter of generating the eigenvectors. Since the system (5.10) is homogeneous and the eliminating determinant vanishes, the eigenvector is determined for each eigenvalue from $N-1$ of the equations by setting one component to unity. The Nth equation then provides a check on both the production of the eigenvectors and the eigenvalues.

In Figure 6 there are plots of several wave functions produced in this manner. All of the wave functions for $N = 50$ are plotted in the top portion. When the eigenfunctions are generated, the values of the intermediate components become quite large, and a multiplicative constant is adjusted so that the largest slope is 20°. This amplitude is a little large for the linear regime and is used solely for exaggeration in the plotting. To interpret Figure 6 the reader must remember that the amplitudes of the eigenfunctions are angles relative to the line joining the Earth and the center of mass of the tether, not the total excursion from that line. Because the same eliminant (5.10) is obtained for both the in-plane and out-of-plane motions, the wave functions are identical; however, the eigenvalues (5.9) are different. The ratios of frequencies are not in general commensurable which means that a tether oscillation composed of two or more eigenfunctions will be a traveling wave with a cork screw motion for combined in- and out-of-plane motions and that any initial wave form eventually loses its coherence to random oscillations.

As noted above the eigenvalues for a given mode of the rosary tether are the same for a tether made up of any number of segments; that is, the eigenvalue for say the $j = 5$th mode is the same whether the tether has 5 or 1000 elements. The

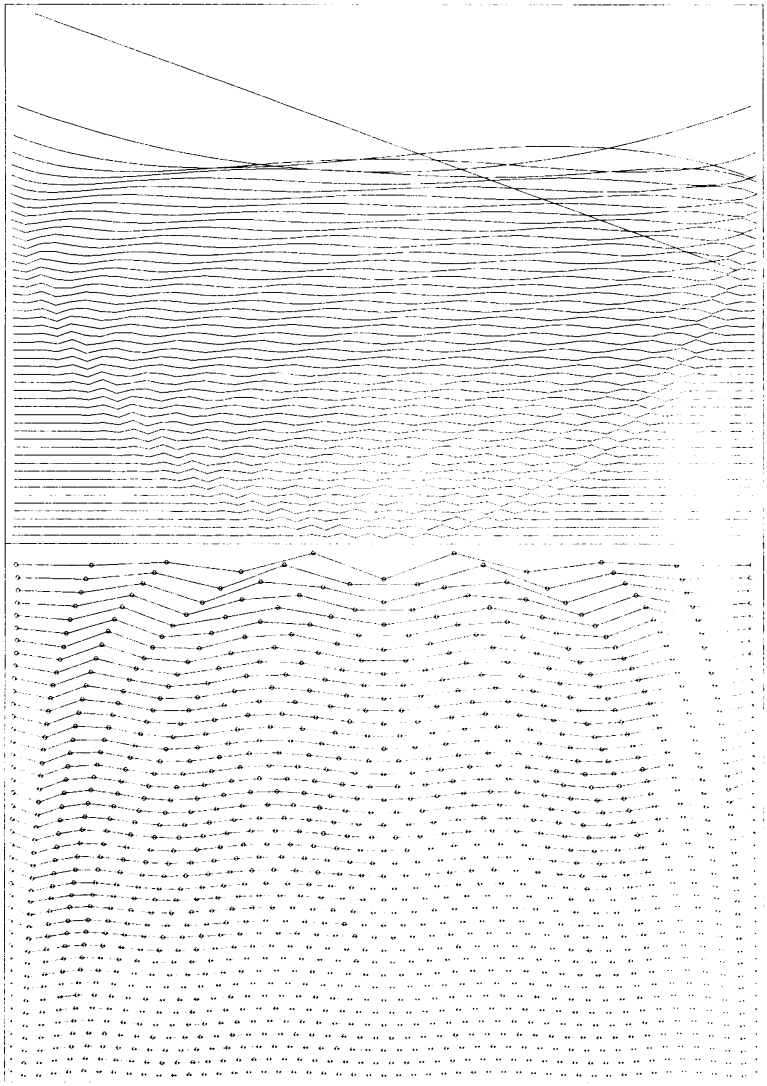

FIG. 6. Standing waves of the rosary tether. All eigenfunctions for a 50 segment tether above, and the 10th mode for tethers of 10 to 50 segments below.

eigenvectors, however, are not the same. As the number of tether segments increases for a given mode, the standard wave makes the transition from a jagged collection of line segments to a smooth curve. This fact is illustrated in the bottom portion of Figure 6 where the $j = 10$ wave functions are plotted for $N = 10, 11, \ldots, 50$. To avoid the confusion of overlapping curves, the center of mass is displaced slightly in Figure 6 for each standing wave. Beyond $j = 1$ and 2 the wave functions are both amplitude and frequency modulated and as such bear a resemblance to Mathieu functions.

Acknowledgments. This paper could not have been completed in a timely manner were it not for the software tools (the fourth-order Runge-Kutta integrator, the spherical projection, and the Euclid reduction of rational fractions) and discussions so kindly supplied by Robert R. Dasenbrock of the Naval Research Laboratory. Mr. Nathan Pillsbury aided in the CRAY programming. This work was supported by Mr. Michael Kaplan of the Naval Research Laboratory under contract sponsored by SDIO/SN.

References

[1] G. W. Hill, *Researches in the Lunar Theory*, in *The collected works of George William Hill*, Carnegie Institute of Washington, Memoir No. 32, 284–335 (1905)
[2] P. C. Hughes, *Spacecraft attitude dynamics*, John Wiley and Sons, New York (1986)
[3] G. D. Birkhoff, *Dynamical systems*, Amer. Math. Soc. Colloquium Publications, New York, Vol. IX (1927)
[4] R. M. Rosenberg, *On the existence of normal mode vibrations of nonlinear systems with two degrees of freedom*, Quart. Appl. Math. **22**, 217–234 (1964)
[5] P. J. Melvin, *On deviations from linear wave motion in inhomogeneous stars*, Quart. Appl. Math. **35**, 75–97 (1977)
[6] R. H. Rand, *A direct method for non-linear normal modes*, Internat. J. Non-Linear Mech. **9**, 363–368 (1974)
[7] L. A. Month and R. H. Rand, *An application of the Poincaré map to the stability of nonlinear normal modes*, J. Appl. Mech. **47**, 645–651 (1980)
[8] G. Pecelli and E. S. Thomas, *Normal modes, uncoupling, and stability for a class of nonlinear oscillators*, Quart. Appl. Math. **37**, 281–301 (1979)
[9] Y. Nejoh, *A nonlinear normal mode in an anharmonic lattice with a single defect*, Physica Scripta **28**, 561–564 (1983)
[10] W. E. Ferguson, H. Flaschka, and D. W. McLaughlin, *Nonlinear normal modes for the Toda chain*, J. Comput. Phys. **45**, 157–209 (1982)
[11] S. Briere, *Nonlinear normal mode initialization of a limited area model*, Mon Weather Rev, **110**, 1166–1186 (1982)
[12] P. J. Melvin, *On the construction of Poincaré–Lindstedt solutions: The nonlinear oscillator equation*, SIAM J . Appl. Math. **33**, No. 1, 161–194 (1977)
[13] R. R. Dasenbrock, *A FORTRAN-based program for computerized algebraic manipulation*, NRL Report 8611, Naval Research Laboratory, Washington, D. C., 1982
[14] A. Deprit and A. Rom, *The main problem of artificial satellite theory for small and moderate eccentricities*, Celestial Mechanics **2**, 166–206 (1970)
[15] T. A. Bray and C. L. Goudas, *Doubly symmetric orbits about the collinear Lagrangian points*, Astron. J. **72**, No. 2 (1967)
[16] R. H. Vassar and R. B. Sherwood, *Formationkeeping for a Pair of Satellites in a Circular Orbit*, J. Guidance, Control and Dynamics **8**, No. 2, 235–242 (1985)
[17] K. R. Symon, *Mechanics*, Second Edition, Addison-Wesley, Reading, Massachusetts, 1960
[18] H. Goldstein, *Classical Mechanics*, Addison-Wesley, Reading, Massachusetts, 1950
[19] P. J. Melvin, *The phase-shifting limit cycles of the van der Pol equation*, J. Res. Nat. Bur. Standards **83**, No. 6, 593–601 (1978)
[20] A. Deprit, *Celestial mechanics: Never say no to a computer*, J. Guidance, Control, and Dynamics **4**, 577–581 (1981)
[21] A. Deprit and D. S. Schmidt, *Exact coefficients of the limit cycle in van der Pol's equation*, J. Res. Nat. Bur. Standards **84**, No. 4, 293–297 (1979)
[22] M. B. Dadfar, J. Geer, and C. M. Andersen, *Perturbation analysis of the limit cycle of the free van der Pol equation*, SIAM J. Appl. Math. **44**, No. 5, 881–895 (1984)
[23] J. V. Breakwell and J. W. Gearhart, *Pumping a tethered configuration to boost its orbit around an oblate planet*, J. Astronaut. Sci. **35**, No. 1 (1987)